

High-Temperature Oxidation of SSIC in Plasma Flows

Torsten Laux*

German Aerospace Center, Institute of Structures and Design, D-70569 Stuttgart, Germany

Within the scope of this work high-temperature oxidation of SSIC was investigated in plasma wind tunnels at the Institute of Space Systems, University of Stuttgart. The tests were performed in both arc heated nitrogen/oxygen plasma flows and inductively heated oxygen plasma flows. In oxygen plasmas, passive-active transitions were determined for temperatures between 1801°C and 1869°C and for oxygen partial pressures between 812 and 3132 Pa. The tests were performed in supersonic and subsonic flows at velocities ranging from 390 to 6000 m/s. Passive-active transitions in nitrogen/oxygen started at temperatures from 1417°C up to 1839°C and oxygen partial pressures between 4 and 160 Pa. Active-passive transitions were determined for surface temperatures between 1831°C and 2145°C at oxygen partial pressures from 28 up to 2290 Pa. The pressures were estimated using mass spectrometer and Pitot probe measurements. The flow velocity was between 1570 and 6500 m/s. Analytical observations show, that reactions at the interface SiC-C-SiO₂ are responsible for the degradation of the silicon dioxide layer. to the active oxidation occurs. The temperature jump during transition from passive to active oxidation in oxygen plasmas is attributed to the reaction of gaseous silicon and atomic oxygen, while the recombination of atomic nitrogen is mainly responsible for this phenomenon in nitrogen/oxygen plasma flows.

Introduction

The high-temperature oxidation of silicon carbide was extensively investigated with regard to the transition between passive and active oxidation in nondissociated atmospheres.¹ Only a few studies were concentrated on the influence of atomic oxygen on the transition.^{2,3} The occurrence of atomic oxygen shifts the transition at constant temperature down to lower oxygen partial pressures. The same applies for the flow velocity.^{4,5} Turkdogan et al⁶ posited a theoretical approach for this behaviour regarding the vaporisation of metals.

In particular, the knowledge when a transition occurs in dissociated atmospheres at very high velocities is important for aerospace applications. Here, SiC or SiC containing materials are applied as antioxidation coating to the parts of the reusable re-entry vehicles, which experience the largest thermal and chemical loads. for the thermally and chemically highest loaded parts of a reusable re-entry vehicle. Hence, nose cap and wing leading edges of such vehicles are built of carbon fiber ceramics, e.g. C/C^{7,8} or C/C-SiC.⁹ Experiments to simulate these loads are performed in so-called plasma wind tunnels.^{10,11}

At the Institute of Space Systems (IRS), University of Stuttgart, the passive-active transition of SiC was first intensively investigated by Hilfer¹² using simulated air flows of high enthalpy. These plasma wind tunnel tests showed that the transition from passive oxidation to the active oxidation is accomplished by a sudden temperature increase of several hundred Kelvin. This and the ongoing mass loss of coating and carbon fiber ceramic pose a risk during re-entry. Thus they are unacceptable for the reusability of space

vehicles.

Figure 1 shows exemplary passive-active transitions, observed at the IRS in magnetoplasmadynamically generated flows using the source RD5.¹⁵ The experiments were performed using sintered silicon carbide (SSIC) or C/C-SiC, coated with SiC by chemical vapor deposition. All data are located in the transition area, which was deduced from volatility diagrams developed by Heuer & Lou.¹⁴ These diagrams are based on thermodynamic equilibrium reactions without considering kinetics. Apart from Rosner & Allendorf's tests in atomic oxygen² all available experimental data are enclosed by the "isomolare line" and the limit for silicon saturated SiC (activity $a_{Si}=1$).¹⁶

Theoretical explanations of the temperature jump in nitrogen/oxygen plasmas were presented both by Hilfer¹² and by Hald.¹⁷ Both found out that atomic nitrogen is playing a main role in the temperature in-

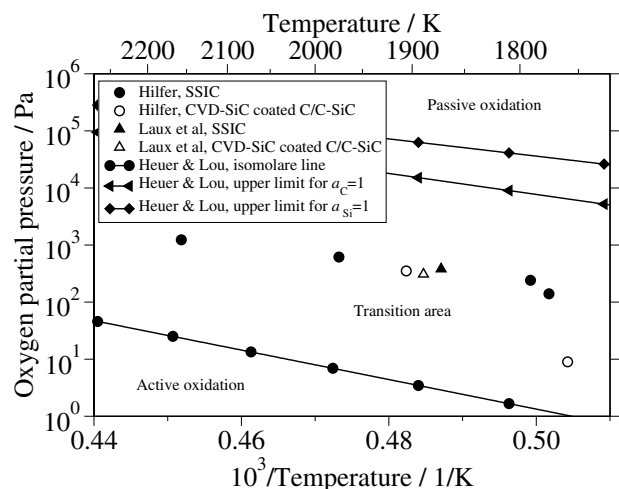


Figure 1 Passive-active transition data in magnetoplasmadynamically generated N₂/O₂ flows; Hilfer,¹² Laux et al,¹³ Heuer & Lou¹⁴

*Research Engineer, Space System Integration

crease. Beside the oxidation of silicon, Hilfer favoured the explanation involving the recombination of two nitrogen atoms to molecular nitrogen. On the other hand, Hald considered silicon as a catalyst passing through two exothermic reactions including formation of molecular nitrogen. Hilfer also proposed a theory for the passive–active transition in plasma flows:



In this paper the experimental studies of the transition between passive and active oxidation of SSIC in oxygen and nitrogen/oxygen plasma flows are presented. The experiments were conducted at the ground test facilities of the IRS. Instead of a magnetoplasma dynamic plasma source, inductively heated and thermal arc plasma generators were used to investigate different dissociation degrees and flow velocities. Furthermore, the passive–active transition is considered analytically.

Experimental Setup

Plasma wind tunnels are facilities that partially recreate re–entry conditions. They are mainly used to qualify thermal protection materials. In general, they consist of a vacuum tank, a pump system to create the low ambient pressure, a plasma source to generate the high enthalpy plasma flow, a suitable power supply system, and the measurement equipment and data processing system (see Fig. 2).

The present study was performed in the arc heated plasma wind tunnel PWK2(4) and the inductively heated PWK3. The water cooled vacuum chamber of PWK2(4) is 5 m in length with a 2 m diameter. The chamber is equipped with a 4-axis positioning system on which the various probes for plasma diagnostic or specimen support systems can be mounted. The test

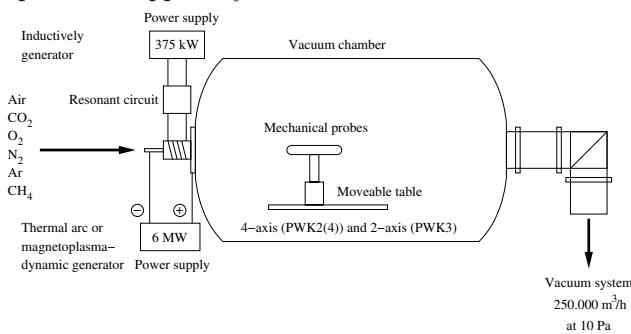


Figure 2 Sketch of the plasma wind tunnels at IRS

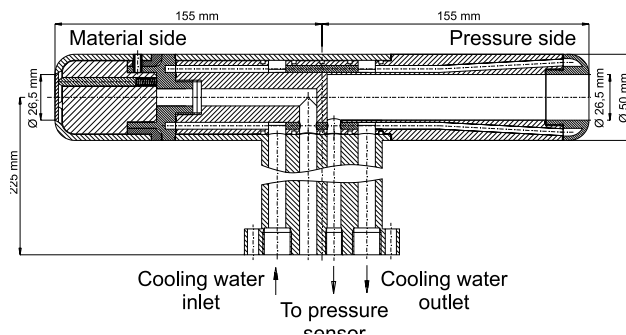


Figure 3 The Material–Pitot pressure–Probe

gas is heated up in the discharge chamber of the coaxial thermal plasma generator RB3 by an electric arc and accelerated in a nozzle. Since contact between the oxygen in the test gas and the cathode has to be avoided, the air plasma has to be simulated. Nitrogen is passed along the cathode into the plenum chamber while oxygen is injected at the downstream end of the anode towards the nozzle throat.¹⁰

PWK3 is about 2 m in length and 1.6 m in diameter. It is equipped with a 2-axis movable table. Inductively heated plasma generators basically consist of an induction coil surrounding a plasma container (tube) and are connected to capacitors. In comparison with arc plasma generators, inductively heated sources generate flows with significantly lower impurity levels because of the absence of electrodes. This is also the case for chemically aggressive gases such as pure oxygen or carbon dioxide. The alternating current in the coil induces a mostly azimuthal electric field inside the quartz tube where an electrical discharge is generated in the test gas.¹⁸ Here, the inductive generator IPG3 was used.

In order to measure and observe the plasma as well as to measure the surface temperatures of material samples, optical access to the vacuum chambers is provided. Both tunnels are connected to a four stage vacuum pump system, that allows pressures down to 10 Pa.¹⁰

The experiments were performed using a double probe (Fig. 3), which allows material tests as well as Pitot pressure measurements in stagnation point configuration. The probe has an outer diameter of 50 mm, while the front diameter of the conic material samples was 26.5 mm. The surface temperatures of the materials were detected by an infrared pyrometer or a linear pyrometer. With the help of a quadrupole mass spectrometer the flow quality, in particular the oxygen partial pressure in the thermal plasmas of the RB3, could be determined.¹⁰

Results

The tests were performed with sintered silicon carbide manufactured by H.C. Starck Ceramics GmbH & Co. KG. Because it contains free carbon, it can be assumed that the SSIC is carbon saturated ($a_C=1$). The conic samples had a thickness of 4 mm. As the emissivity of this SSIC was unknown, ϵ was set to 0.8 based on the experiences made at the IRS with this material. Possible changes of the emissivity due to the oxidation were neglected.

Experiments in Oxygen Plasma Flows

The tests were performed in the inductively heated plasma wind tunnel PWK3. Here, only oxygen was heated up to a plasma. The tests were done at six different levels of the chamber pressure p_{ch} controlled by the vacuum system. The oxygen mass flow was 2 g/s ($p_{ch}=40$ Pa) or 3 g/s ($p_{ch} \geq 250$ Pa). After setting the test conditions, i.e. chamber pressure, mass flow and anode voltage, the probe is moved into the symmetry axis of the plasma flow (y -position=0 mm) at a thermally uncritical distance (x -position). Then, the probe

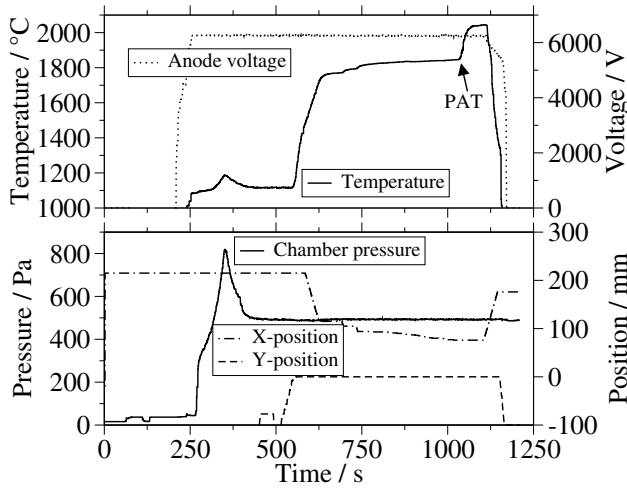


Figure 4 Oxygen plasma flow test data at $p_{ch}=500$ Pa

Table 1 Passive-active-transitions in oxygen plasma flows

p_{ch} Pa	ϑ^{PAT} °C	p_{O_2+O} Pa	v_∞ m/s
40	1869±6	812±47	6052±1614
250	1851±8	902±51	2389±637
500	1847±7	1186±66	1830±488
1000	1853±6	1598±82	1309±349
2000	1801±6	2267±116	663±177
3000	1815±6	3132±167	387±103

is moved step by step closer to the generator exit. This leads to higher surface temperatures. At a certain x-position a sudden significant temperature increase occurs. In the test depicted in Fig. 4 the surface temperature increased from 1847°C to 2044°C. Comparable temperature differences between passive and active oxidation were determined for the other chamber pressures (174K to 249K). The respective Pitot pressures equal to the oxygen partial pressures were measured in separate experiments. The determined passive-active transitions are listed in Table 1.

All transitions occurred in a very small temperature range of about 70 K. This fact confirms transitions determined in earlier experiments when SSIC of a different manufacturer was used.¹⁹ Again a strong dependence on the velocity could be determined. The flow velocity v_∞ of the undisturbed flow can be calculated from the speed of sound a_∞ and the Mach number M_∞ :

$$v_\infty = M_\infty \cdot a_\infty . \quad (2)$$

For the determination of M_∞ , different equations have to be used for subsonic or supersonic flows. In case of subsonic flows the following equation is used:

$$\frac{p_0}{p_\infty} = \left(1 + \frac{\kappa - 1}{2} \cdot M_\infty^2 \right)^{\frac{\kappa}{\kappa - 1}} \quad (3)$$

with κ as the isentropic exponent. In case of a supersonic flow, a shock is formed in front of the probe. Here, a significant increase of density, temperature and



Figure 5 SSIC-sample and cap after test in oxygen plasma flow at $p_{ch}=3000$ Pa

pressure appear and the velocity turns from supersonic to subsonic behind the shock. The Mach number M_∞ can be calculated iteratively from:

$$\frac{p_0}{p_\infty} = \left(\frac{\kappa + 1}{2} \cdot M_\infty^2 \right)^{\frac{\kappa}{\kappa - 1}} \cdot \left(\frac{2 \cdot \kappa}{\kappa + 1} \cdot M_\infty^2 - \frac{\kappa - 1}{\kappa + 1} \right)^{\frac{1}{1 - \kappa}} . \quad (4)$$

In both flows the ratio of the pressure at the stagnation point p_0 to pressure in the flow p_∞ is approximately the ratio of the measured Pitot pressure to the chamber pressure:

$$\frac{p_0}{p_\infty} \approx \frac{p_{Pitot}}{p_{ch}} . \quad (5)$$

For $\kappa=1.1, \dots, 1.6$ the ratio is between 1.7 and 2 at $M_\infty=1$. For oxygen flows, a speed of sound of 1500 m/s and $\kappa=1.3$ was used. These values were assumed for a mean plasma temperature between 3500 K and 4000 K.¹⁶ At these temperatures oxygen is almost fully dissociated. As listed in Table 1, the flow velocity decreased from 6052 m/s at 40 Pa chamber pressure down to 387 m/s at 3000 Pa. This dramatic change is due to the characteristic behaviour of the inductive generator. Between 500 and 1000 Pa the flow drops from supersonic to subsonic condition.

Here also, a slight difference in heat flux measurements, which were performed on various surfaces, was detected. These measurements led to the assumption that the degree of dissociation of oxygen was a tad lower at $p_{ch} \geq 1000$ Pa.¹⁶

Figure 5 shows the typical appearance of a sample after an active oxidation. The surface changed from smooth to rough. Beside the SSIC sample, the cap was also oxidised actively. A few of the samples were analysed by X-ray diffraction (XRD), scanning electron microscopy (SEM) and energy dispersive X-ray analysis (EDX). A SEM micrograph of the sample tested at 3000 Pa is seen in Fig. 6. The surface is partially covered with a layer containing a lot of bubbles. Based on the EDX analysis (Fig. 7) of this layer, on which

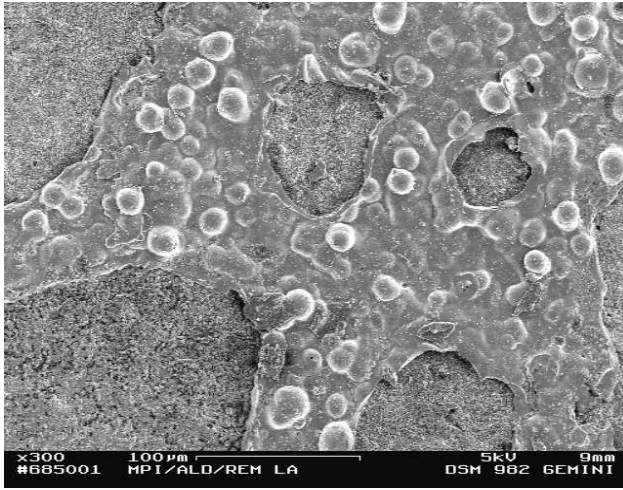


Figure 6 SEM micrograph in the middle of the sample actively oxidised in oxygen plasma flow at $p_{ch}=3000$ Pa

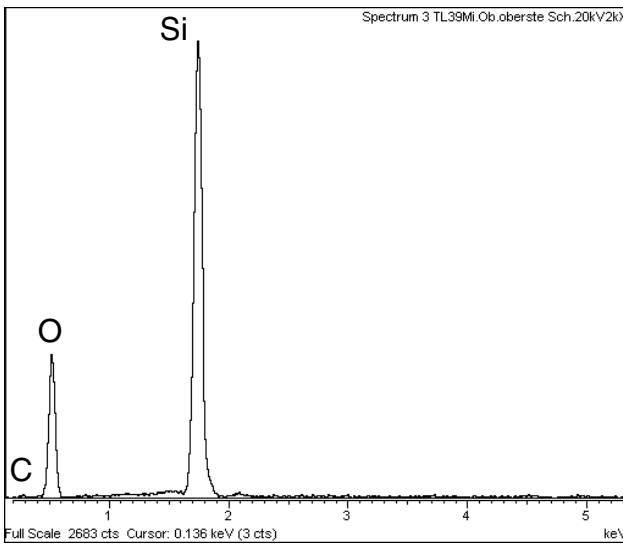


Figure 7 EDX analysis of the bubble containing layer in Fig. 6

mainly the elements silicon and oxygen were identified, the cover is silicon dioxide. Similar results were found on the other samples. The samples are layered with SiO_2 . A lot of closed and burst bubbles could be observed. Using XRD diffraction, no crystalline structure could be detected. Therefore, it is assumed that the layer consists of amorphous silicon dioxide.

Experiments in Nitrogen/Oxygen Flows

The basic approach of the tests in the thermal arc flows was to detect passive-active transitions in simulated air for the first time. After a few experiments it was established that the oxygen partial pressure was too high and the enthalpy was too low to achieve transitions. Therefore a different procedure was performed. First, the samples are heated up in nitrogen. This means that only nitrogen is injected into the plasma generator.

Figure 8 shows a test at $p_{ch}=500$ Pa. As in oxygen flows at a certain x-position, a significant temperature increase occurs. Afterwards the oxygen mass flow is increased in small steps until a sudden temperature drop to the starting point is reached. This decrease

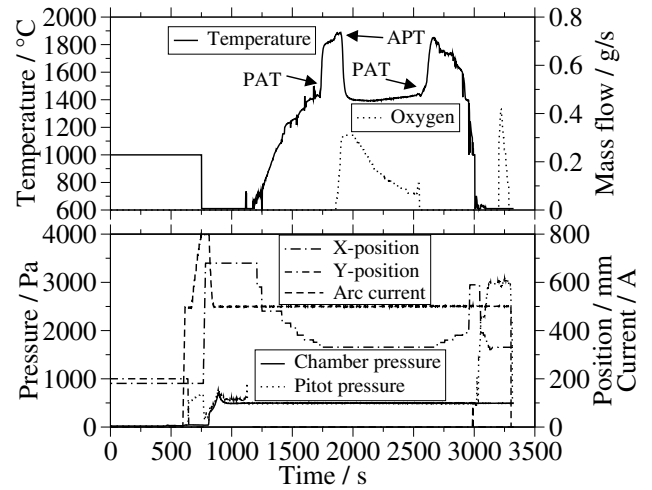


Figure 8 Test in nitrogen/oxygen plasma flow at $p_{ch}=500$ Pa

Table 2 Passive-active-transitions in nitrogen/oxygen plasma flows; [¶] identical test as in Table 3 at same p_{ch} , *based on mass spectrometer measurements, [°] estimation

p_{ch} Pa	ϑ^{PAT} °C	p_{O_2+O} Pa	p_{Pitot} Pa	v_∞ m/s
50 [¶]	1560±16	4*	1028±53	6483±1729
50	1790±19	18*	973±51	6303±1681
50	1568±20	10 [°]	745±45	5493±1465
50	1641±18	30 [°]	1600±80	8124±2166
400	1839±20	160 [°]	6134±355	5575±1487
500 [¶]	1446±25	7*	2976±191	3375±900
500 [¶]	1442±15	7*	2976±191	3375±900
1000 [¶]	1417±14	48*	4381±261	2842±758
2000	1470±29	22 [°]	7372±432	2570±685
2000 [¶]	1520±25	22 [°]	6285±356	2334±622
3000 [¶]	1583±16	13*	7095±394	1939±517
4000 [¶]	1571±20	22 [°]	8105±468	1732±462
5000 [¶]	1544±15	22 [°]	8780±506	1537±410

is connected to an active-passive transition never before detected in plasma wind tunnels at the IRS. In the case of the shown test, even the passive-active transition could be rebuilt. Again, without any oxygen flow through the generator a temperature increase took place. This led to the question where the oxygen, that is chemically necessary for active oxidation, is coming from. Finally, the vacuum system was found to be responsible for the oxygen in the plasma flow. This was already observed by Fasoulas, who investigated magnetoplasmadynamic generated flows at IRS with a solid electrolyte sensor.²⁰ When the pump system has to work at pressure levels higher than minimum ($p_{ch}>50$ Pa), a set of valves is opened for the inlet of additional air. Now air or oxygen can diffuse in the direction of the mass flow. Inside the chamber the oxygen is mixed partially with the plasma flow.

The unknown oxygen pressures p_{O_2+O} were partially determined by the described mass spectrometry. The missing ones were assumed.¹⁶ As for the inductive ex-

Table 3 Active–passive–transitions in nitrogen/oxygen plasma flows; *based on mass spectrometer measurements, °estimation

p_{ch} Pa	ϑ^{APT} °C	p_{O_2+O} Pa	p_{Pitot}	v_∞ Pa m/s
50	1912±19	28*	1110±57	6743±1798
500	1850±19	48*	2295±202	3387±903
1000	1831±39	167*	4383±236	2843±758
2000	1900±19	920°	6144±333	2230±595
3000	2000±20	1712*	7331±468	1923±513
4000	2145±21	1730°	8686±549	1767±472
5000	1976±39	2290°	9626±545	1612±430

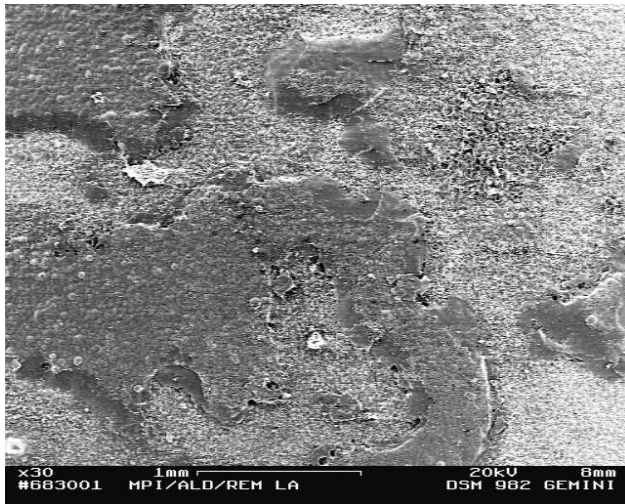


Figure 9 SEM micrograph of the sample, actively oxidised in nitrogen/oxygen at $p_{ch}=2000$ Pa

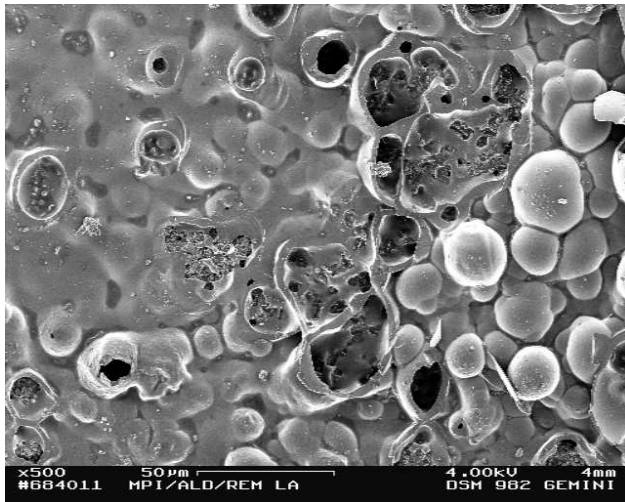


Figure 10 SEM micrograph of the sample, actively oxidised in nitrogen/oxygen at $p_{ch}=2000$ Pa

periments with oxygen plasma, the flow velocities were calculated using equations 2 to 4. For these calculations, a speed of sound of 1500 m/s and an isentropic exponent of 1.1 or 1.2 were used. These properties were based on a mean temperature of nitrogen plasma between 5000 and 6000 K. This temperature range was estimated from heat flux measurements followed by enthalpy calculations according to Pope's theory.²¹ All

flows are supersonic while the velocity decreases with increasing chamber pressure.¹⁶

Figures 9 and 10 show SEM micrographs of the sample tested at $p_{ch}=2000$ Pa. Both covered and uncovered areas can be seen (Fig. 9). It is assumed that the active oxidation does not remove the SiO_2 layer from the surface due to active oxidation. Again, the surface contains a lot of closed and burst bubbles (Fig. 10).

Discussion

Passive–Active Transition in Plasma Flows

As already mentioned, Hilfer¹² assumed, that the silicon dioxide layer is removed because of its reaction with atomic oxygen (Eq. 1). In fact, the SEM micrographs disagree with that. There are areas with SiO_2 on the surface of actively oxidised samples (see Fig. 6). Hence it can be concluded, that non–uniform layer degradation occurs. The areas of silicon dioxide were formed during the passive oxidation before the transition started. In the experiments the active oxidation runs at temperatures above the melting point of silicon dioxide (1723°C) where it is liquid or viscous but stable.

Furthermore, a lot of bubbles are located in the remaining silicon dioxide layers (Fig. 9). The bubble formation is connected to the formation of SiO and CO. If you take a look at the cross section in Fig. 11, the location of the bubble formation starting point can be identified. Bubbles are formed at the interface between SiC and SiO_2 . Free carbon could also be involved as we assume that the tested SiC is carbon saturated.

The transition from passive to active oxidation in plasma flows can be imagined as follows. It starts with bubble formation at the interface. If the pressure inside the bubbles is greater than the outer pressure, the bubbles burst. This leads to spallation of parts of the layer. It is possible that some silicon dioxide reacts according to Hilfer's proposition (Eq. 1), but the main reaction zone for the transition is at the interface SiC–C– SiO_2 . As the transition data were detected in wide

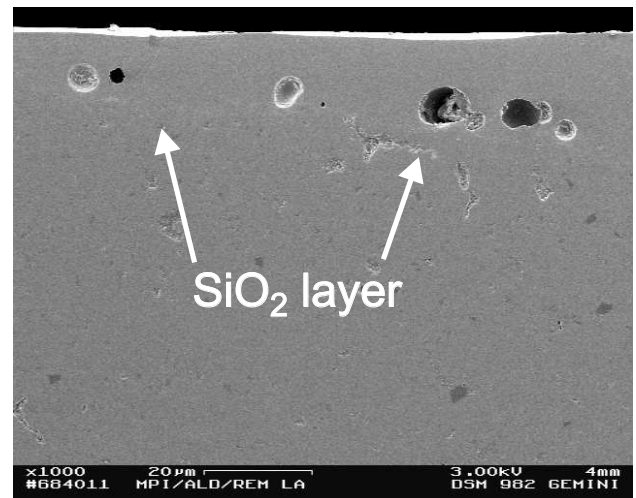


Figure 11 SEM cross section of actively oxidised sample nitrogen/in oxygen at $p_{ch}=5000$ Pa

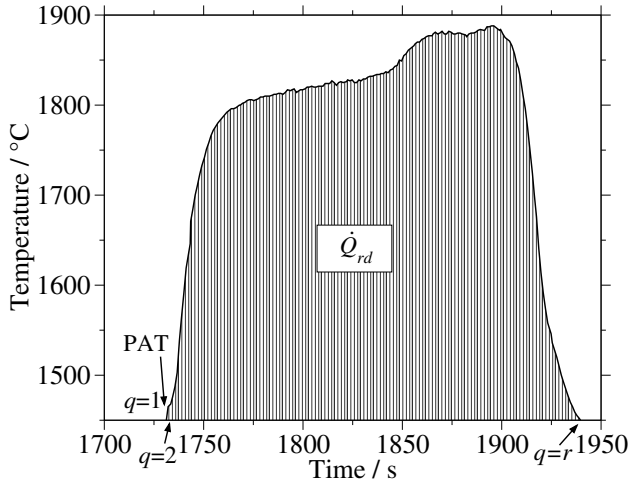


Figure 12 Estimation of heat radiation

range of temperature and oxygen partial pressure, it is not possible to explain the transition with one single reaction. A set of reactions must be responsible for the transition as suggested in the model of Heuer & Lou.

Temperature Jump

After the burst of the bubbles, the known significant temperature increase occurs. An energy balance is established to determine the responsible reactions. To simplify the analysis, the nonequilibrium of the plasma is neglected. It is assumed that the change of the convective heat flux as well as of the conductive heat flux can be neglected.¹⁶ Including these considerations, a balance between radiation heat and reaction enthalpy can be established:

$$Q_{rd} = \Delta_r H^{\text{PAT}} . \quad (6)$$

The radiation heat is calculated by:

$$Q_{rd} = \sum_{q=2}^r \varepsilon \sigma A \left(T^{\text{PAT}4} - T_q^4 \right) (t_q - t_{q-1}) . \quad (7)$$

This is the step-wise summation of the heat, which is radiated in the time $t_q - t_{q-1}$ until $t_q = t_r$ is reached (see Fig. 12). The reaction enthalpy is calculated in a similar way:

$$\Delta_r H^{\text{PAT}} = \sum_{o=1}^p \left[\sum_{q=2}^r \bar{n}_o \Delta_r h_q (t_q - t_{q-1}) \right] \quad (8)$$

with the molar reaction enthalpy $\Delta_r h$:

$$\Delta_r h_q = \sum_{i=1}^n \nu_i \left(\Delta_b h_i^\circ + \int_{T^\circ}^{T_q} c_{p,i} dT \right) . \quad (9)$$

The enthalpy of a single reaction is calculated by the standard enthalpy of formation $\Delta_b h^\circ$ and the specific heat capacity c_p . The average mole flow \bar{n}_o of a reaction p is estimated by the mass loss during active oxidation Δm^{AO} , the time of active oxidation t^{AO} and a chosen factor, which weighted the respective reaction.

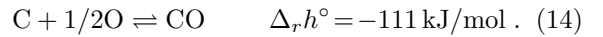
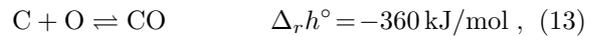
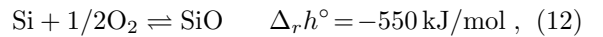
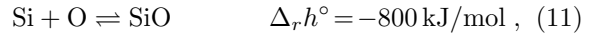
Table 4 Specific mass loss of SSIC during active oxidation, test duration, temperature difference, heat radiation

Plasma	p_{ch} Pa	Δm^{AO} g	t^{AO} s	ΔT^{PAT} K	Q_{rd} kJ
N ₂ /O ₂	500	0.13229	566	393	-106.7
N ₂ /O ₂	1000	0.42030	346	468	-101.8
N ₂ /O ₂	2000	2.15018	269	455	-99.5
N ₂ /O ₂	3000	1.90729	214	516	-91.4
N ₂ /O ₂	5000	1.19534	178	469	-60.2
O ₂	40	1.49254	82	174	-12.3
O ₂	500	2.06244	93	197	-14.8
O ₂	1000	2.25166	88	249	-18.5
O ₂	2000	2.52273	118	234	-15.2
O ₂	3000	2.37704	120	191	-15.0

In the following, reactions, which already were considered by Hilfer¹² and Hald,¹⁷ are introduced. The first one is the decomposition of silicon carbide:

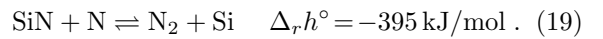
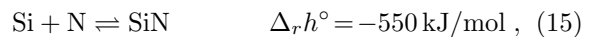


It is assumed that the decomposition starts just after the SiO₂ layer is removed from the surface. Afterwards, silicon and carbon can react with atomic or molecular oxygen:

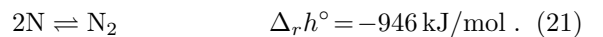
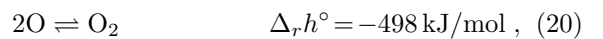


The reactions 11, 12 and 14 were also included in the analyses by Hilfer and Hald.

If there is atomic nitrogen in the flow, the following reactions may happen:



Reactions 15 and 19 represent the conception of Hald¹⁷ (see Introduction). Furthermore, recombination reactions, as done by Hilfer,¹² are considered:



Beside a temperature increase, the active oxidation is often accompanied by a green emittance in front of the probe and around the sample support system, the SSIC cap. Boubert and Vervisch allocated C₂ for that appearance. They expressed the following reaction:²²



Table 5 Examples of the energy balance according to Eq. 8

Substance	Reaction o	\bar{n}_o mmol/s	$\Delta_r H$ kJ	Substance	Reaction o	\bar{n}_o mmol/s	$\Delta_r H$ kJ
Oxygen, $p_{ch}=2000$ Pa				$Q_{rd}=-15.2$ kJ			
Case 1				Case 2			
SiC	Eq. 10	0.537	32.6	SiC	Eq. 10	0.537	32.6
Si	Eq. 11	0.537	-51.3	Si	Eq. 11	0.537	-51.3
C	Eq. 13	0.242	-10.8	C	Eq. 13	0.269	-12.0
C	Eq. 23	0.295	14.3	C	Eq. 22	0.219	15.5
			Σ				Σ
			-15.2				-15.2
Nitrogen/Oxygen, $p_{ch}=3000$ Pa				$Q_{rd}=-91.4$ kJ			
Case 3				Case 4			
SiC	Eq. 10	0.222	24.6	SiC	Eq. 10	0.222	24.6
Si	Eq. 11	0.222	-38.8	Si	Eq. 15	0.222	-26.5
C	Eq. 13	0.222	-18.1	C	Eq. 13	0.222	-18.1
			Σ	SiN	Eq. 19	0.222	-18.6
			-32.3				Σ
							-38.6

This reaction follows the formation of CO according the Eqs. 13 and 14. Another possible formation could be the direct reaction of two carbon atoms:



First, the test in pure oxygen at a chamber pressure of 2000 Pa is considered. Here, a radiation heat of -15.2 kJ was emitted (Table 4). While the total mass loss of 2.52273 g is connected to the loss of silicon carbide, an average mole flow of 0.527 mmol/s is calculated. According to reaction 10, SiC is decomposed into Si and C by an enthalpy consumption of 32.6 kJ (Table 5). Next, it is assumed that all silicon ($\bar{n}_{Si}=0.537$ mmol/s) reacts with atomic oxygen to form SiO, while releasing an reaction enthalpy of 51.3 kJ. In the case of carbon, the formation of C_2 is considered. All tests were accompanied by a significant green emittance. Two cases (case 1 and 2) are calculated because two ways of formation are possible. In case 1, a part of carbon reacts according to Eq. 23. The rest oxidises with atomic oxygen while the values of both average mole flows are chosen to fulfill the energy balance (Eq. 6). Beside the CO formation, in case 2 carbon reacts according to Eq. 22. The recombination of O-atoms, which disposes a high reaction enthalpy, has not to be considered in the balance because the formation of SiO provides sufficient enthalpy to explain the temperature increase in oxygen plasma flows.

In contrast to that, in nitrogen/oxygen the mass losses during active oxidation are lower but the radiation heat is significantly higher than in oxygen (see Table 4). The temperature jump in N_2/O_2 was between 393 K and 516 K, while in oxygen a maximum temperature increase of 249 K was measured. For example, a radiation heat of -91.4 kJ was emitted during the active oxidation at 3000 Pa. Again, it is assumed that all SiC is decomposed with an average mole flow of 0.222 mmol/s. If both silicon and carbon is oxidised with atomic oxygen, the total enthalpy of the three reactions results in -32.3 kJ, which is about the third of the radiation heat. Case 4 considers the role of atomic

nitrogen. While carbon is oxidised to CO, silicon reacts with atomic nitrogen to SiN. Hereafter, silicon nitride reacts with N and the catalyst silicon is released. According to Hald silicon passes through these two reactions until the energy balance is fulfilled. Example 4 in Table 5 only included one pass, whereas an enthalpy of -38.6 kJ is released totally. Silicon must pass the reactions at least two times to equalize the balance. Because of the high flow velocities in front of the probe, this process is questionable.

The recombination of nitrogen (Eq. 21) is more suitable to explain the temperature increase in nitrogen/oxygen plasmas. It is a direct reaction with a high reaction enthalpy independent whether the recombination follows the Eley-Rideal or the Langmuir-Hinshelwood mechanism. Figure 13 shows the recombination efficiencies of oxygen and nitrogen on SiO_2 and SiC. Both the nitrogen recombination and the oxygen recombination on silicon dioxide is orders of magnitude lower compared to those on SiC. That means, if the SiO_2 layer is removed from the surface, even partially, more nitrogen atoms can recombine, which leads to a higher release of reaction enthalpy $\Delta_r H$.

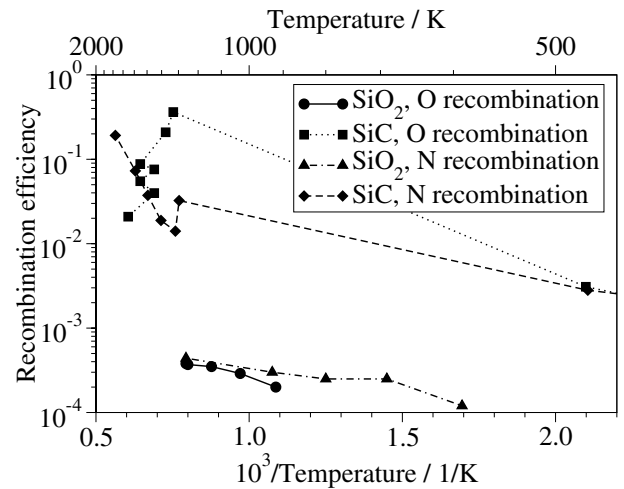


Figure 13 Recombination efficiencies, Refs.: SiO_2 ,²³ SiC ²⁴

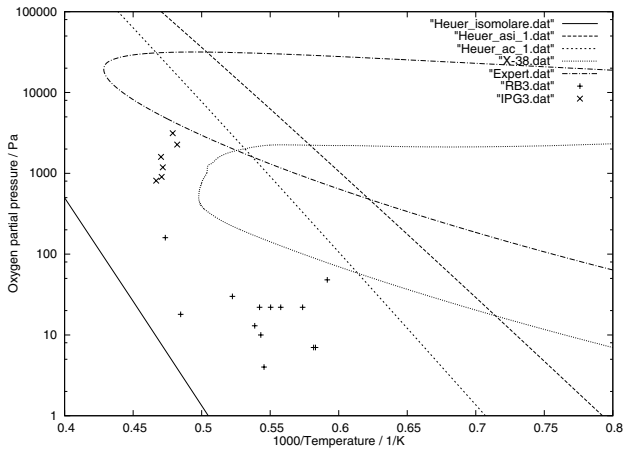


Figure 14 Transition data in comparison with X-38 trajectory²⁵ and EXPERT trajectory, pressure vs. temperature

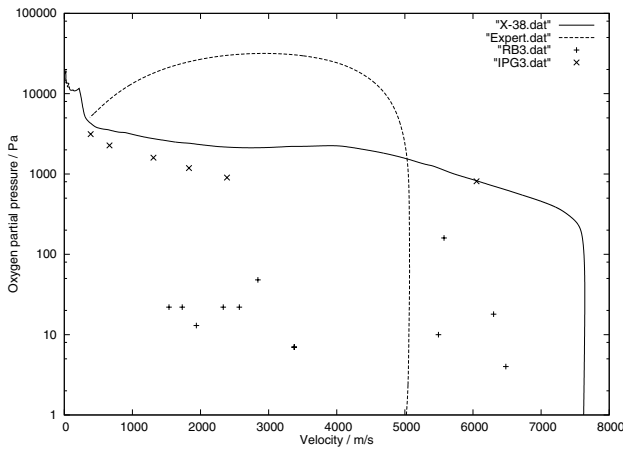


Figure 15 Transition data in comparison with X-38 trajectory²⁵ and EXPERT trajectory, pressure vs. velocity

The amount of nitrogen, which recombines to fulfill the energy balance, is not considered. However, the present analysis confirms Hilfer's explanation of the temperature increase in nitrogen/oxygen.

Extrapolation to Flight

Figure 14 compares the detected passive-active transitions with the trajectories of X-38²⁵ and EXPERT in a normally used Arrhenius-plot. Both trajectories enter the range of transition predicted by Heuer & Lou. Looking at the IPG3 data, the diagram predicts that the datapair with highest oxygen partial pressure is the simulation of an EXPERT re-entry condition. But here the influence of the velocity is not visible. Plotting oxygen partial pressure vs. velocity we obtain the diagram shown in Fig. 15. Now the IPG3 transitions determined in pure oxygen plasmas seem to better fit to the X-38 trajectory. To visualise both temperature and velocity, a 3d-plot was set-up (Fig. 16). Using such diagrams the extrapolation of test data concerning passive-active oxidation is more meaningful than 2d-Arrhenius-plots of oxygen partial pressure and temperature. Nevertheless, the evaluation of the test in comparison to flight is still hard due to missing real re-entry data with transition.

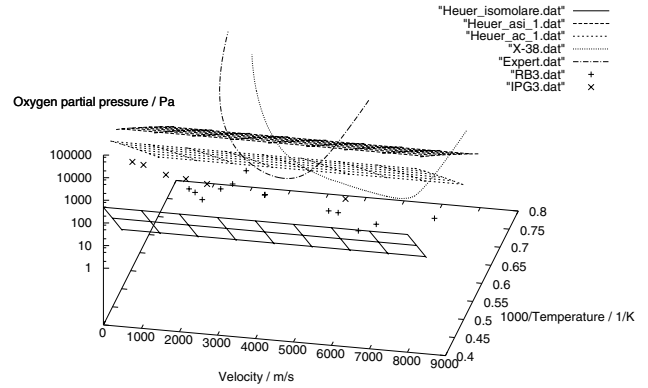


Figure 16 Transition data in comparison with X-38 trajectory²⁵ and EXPERT trajectory, pressure vs. temperature and velocity

Conclusions

Within this study, samples of sintered silicon carbide were passively and actively oxidised in nitrogen/oxygen as well as in oxygen plasma flows. Six passive-active transitions could be detected in oxygen ($\vartheta^{\text{PAT}}=1801\text{--}1869^\circ\text{C}$, $p_{\text{O}_2}=812\text{--}3132\text{ Pa}$) and thirteen in nitrogen/oxygen ($\vartheta^{\text{PAT}}=1417\text{--}1839^\circ\text{C}$, $p_{\text{O}_2}=4\text{--}160\text{ Pa}$). Furthermore, seven active-passive transitions were determined ($\vartheta^{\text{PAT}}=1831\text{--}2145^\circ\text{C}$, $p_{\text{O}_2}=28\text{--}2290\text{ Pa}$). Selected samples were investigated using X-ray diffractometry, scanning electrons microscopy and energy dispersive X-ray analysis. Amorphous silicon dioxide was found on both the actively oxidised and exclusively passively oxidised samples. The partial appearance of silicon dioxide on the surface of actively oxidised samples lead to the conclusion that the theory of Hilfer, which describes the decomposition of the SiO_2 layer due to a reaction with atomic oxygen, is not the reason for decomposition. In fact, reactions at the interface SiC-C-SiO_2 with formation of CO and SiO are responsible for this effect.

With inclusion of the temperature changes, which occurred and the mass losses that resulted during the transition, an analysis was performed to explain the reactions responsible for the temperature jump. For oxygen flows, the reaction of gaseous silicon with atomic oxygen was found to be the reason. The analysis of the transition in oxygen included the formation of C_2 , which seems to be responsible for the appearance of a green emittance during active oxidation. The temperature jumps in nitrogen/oxygen flows, which were greater than those in pure oxygen, result mainly from the recombination of atomic nitrogen.

The influence of the flow velocity on the transition could be shown in the experiments. A 3d-plot was presented, which shows the oxygen partial both vs. temperature and velocity. This illustration is more useful for the extrapolation of test data to flight than a 2d-Arrhenius-plot.

Acknowledgements

All experiments were performed at facilities of the Institute of Space Systems, Stuttgart University. The author thanks all at the IRS for their great support. For the post analysis done at PML (Pulvermetallur-

gisches Laboratorium) of the Max-Planck-Institut für Metallforschung in Stuttgart, the author have to thank Prof. Fritz Aldinger and his staff.

Nomenclature

a	speed of sound	m/s
M	Mach number	—
m	weight	g
\dot{n}	mole flow	mmol/s
p	pressure	Pa
Q_{rd}	radiation heat	kJ
T	temperature	K
t	time	s
v	flow velocity	m/s
y	mole fraction	—
$\Delta_r H$	reaction enthalpy	kJ
ε	emissivity	—
ϑ	temperature	°C
κ	isentropic exponent	—

Superscripts

AO	active oxidation
APT	active-passive transition
PAT	passive-active transition

Subscripts

0	stagnation point
ch	chamber
$Pitot$	total
∞	free stream

References

- Narushima, T., Goto, T., Hirai, T., and Iguchi, Y., "High-Temperature Oxidation of Silicon Carbide and Silicon Nitride," *Mater. Trans., JIM*, Vol. 38, No. 10, 1997, pp. 821–835.
- Rosner, D. E. and Allendorf, H. D., "High Temperature Kinetics of the Oxidation and Nitridation of Pyrolytic Silicon Carbide in Dissociated Gases," *J. Phys. Chem.*, Vol. 74, No. 9, 1970, pp. 1829–1839.
- Balat, M. J., "Determination of the Active-to-Passive Transition in the Oxidation of Silicon Carbide in Standard and Microwave-Excited Air," *J. Europ. Ceram. Soc.*, Vol. 16, 1996, pp. 55–62.
- Vaughn, W. L. and Maahs, H. G., "Active-to-Passive Transition in the Oxidation of Silicon Carbide and Silicon Nitride in Air," *J. Am. Ceram. Soc.*, Vol. 73, No. 6, 1990, pp. 1540–1543.
- Narushima, T., Goto, T., Iguchi, Y., and Hirai, T., "High-Temperature Active Oxidation of Chemically Vapor-Deposited Silicon Carbide in the Ar-O₂ Atmosphere," *J. Am. Ceram. Soc.*, Vol. 74, No. 10, 1991, pp. 2583–2586.
- Turkdogan, E., Grieveson, P., and Darken, L., "Enhancement of Diffusion-Limited Rates of Vaporization of Metals," *J. Phys. Chem.*, Vol. 67, 1963, pp. 1647–1654.
- Curry, D. M., "Space Shuttle Orbiter Thermal Protection System Design and Flight Experience," *1st ESA/ESTEC Workshop on Thermal Protection Systems*, ESA/ESTEC, Noordwijk, 1993.
- Timoshenko, V., "Design and Experimental Development of the BURAN Thermal Protection," *Aerospace Systems: Book of Technical Papers*, edited by Lozino-Lozinsky, G.E. ;

Bratukhin, A.G., Publishing House of Moscow Aviation Institute, 1997, pp. 123–136.

⁹Hald, H. and Weihs, H., "Development of a CMC Nosecap System for X-38," *1st International Symposium: Atmospheric Reentry Vehicles and Systems*, AAAF, Arcachon, 1999.

¹⁰Auweter-Kurtz, M. and Wegmann, T., "Overview of IRS Plasma Wind Tunnel Facilities," *Measurement Techniques for High Enthalpy and Plasma Flows*, RTO/NATO, 2000.

¹¹Gülhan, A. and Esser, B., "Arc-Heated Facilities LBK as a Tool to Study Aerothermodynamic Problems of Reentry Vehicles," *Progress in Astronautics and Aeronautics Series – Advanced Hypersonic Test Facilities*, edited by F. K. Lu and D. E. Marren, Vol. 198, AIAA, 2002.

¹²Hilfer, G., *Experimentelle und theoretische Beiträge zur Plasma-Wand-Wechselwirkung keramischer Hitzeschutzmaterialien unter Wiedereintrittsbedingungen (Experimental and Theoretical Contributions to the Plasma-Wall-Interaction of Ceramic Thermal Protection Materials under Re-entry Conditions)*, Doctoral thesis, University of Stuttgart, 1999.

¹³Laux, T., Ullmann, T., Auweter-Kurtz, M., Hald, H., and Kurz, A., "Investigations of Thermal Protection Materials along an X-38 Re-entry Trajectory by Plasma Wind Tunnel Simulations," *2nd International Symposium: Atmospheric Reentry Vehicles and Systems*, AAAF, Arcachon, 2001.

¹⁴Heuer, A. H. and Lou, V. L., "Volatility Diagrams for Silica, Silicon Nitride, and Silicon Carbide and Their Application to High-Temperature Decomposition and Oxidation," *J. Am. Ceram. Soc.*, Vol. 73, No. 10, 1990, pp. 2789–2803.

¹⁵Auweter-Kurtz, M., Kurtz, H., and Laure, S., "Plasma Generators for Re-entry Simulation," *J. Propul. Power*, Vol. 12, No. 6, 1996, pp. 1053–1061.

¹⁶Laux, T., *Untersuchungen zur Hochtemperaturoxidation von Siliziumkarbid in Plasmaströmungen (Investigations of the High-temperature Oxidation of Silicon Carbide in Plasma Flows)*, Doctoral thesis, University of Stuttgart, 2004.

¹⁷Hald, H., *Faserkeramiken für heiße Strukturen von Wiedereintrittsfahrzeugen — Simulation, Test und Vergleich mit experimentellen Flugdaten (Fibre Ceramics for Hot Structures of Re-entry Vehicles — Simulation, Test and Comparison with Experimental Flight Data)*, Doctoral thesis, University of Stuttgart, 2001.

¹⁸Herdrich, G., Auweter-Kurtz, M., Kurtz, H., Laux, T., and Winter, M., "Operational Behavior of Inductively Heated Plasma Source IPG3 for Entry Simulations," *J. Thermophys. Heat Tr.*, Vol. 16, No. 3, 2002.

¹⁹Laux, T. and Auweter-Kurtz, M., "Investigation of Inductively Generated Oxygen Plasmas using Various Heat Flux Sensors," *35th AIAA Thermophysics Conference*, AIAA, Anaheim, CA, 2001.

²⁰Fasoulas, S., *Experimentelle und theoretische Charakterisierung einer hochenthalpen Stickstoffströmung zur Wiedereintrittssimulation (Experimental and Theoretical Characterisation of a High Enthalpy Nitrogen Flow for Re-entry Simulation)*, Doctoral thesis, University of Stuttgart, 1995.

²¹Pope, R. B., "Stagnation-Point Convective Heat Transfer in Frozen Boundary Layers," *AIAA J.*, Vol. 6, No. 4, 1968, pp. 619–626.

²²Boubert, P. and Vervisch, P., "Laser-Induced Fluorescence Measurements of a³II Metastable Carbon Monoxide in a High Enthalpy Flow," *Eur. Phys. J. D*, Vol. 17, No. 1, 2001, pp. 43–48.

²³Kim, Y. C. and Boudart, M., "Recombination of O, N, and H Atoms on Silica: Kinetics and Mechanism," *Langmuir*, Vol. 7, 1991, pp. 2999–3005.

²⁴Stewart, D. A., "Determination of Surface Catalytic Efficiency for Thermal Protection Materials — Room Temperature to Their Upper Use Limit," *31st AIAA Thermophysics Conference*, AIAA, New Orleans, LA, 1996.

²⁵Tigges, M., "Preliminary V-201 Entry Flight Profile with Landing Site Precision. Cycle 8," Technical report, NASA, October 1998.